POLITECNICO
MILANO 1863

DIPARTIMENTO DI MECCANICA

mecc

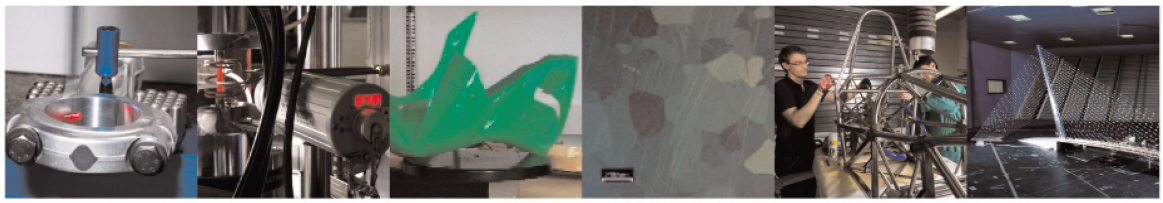

On the Implementation of Hydraulic-Interconnected-Suspensions at the Primary Suspension Stage of High-Speed Rail Vehicles

Gioele Isacchi and Francesco Ripamonti

DIPARTIMENTO DI MECCANICA ■ POLITECNICO DI MILANO
via G. La Masa, 1 ■ 20156 Milano ■ EMAIL (PEC): pecmecc@cert.polimi.it
http://www.mecc.polimi.it

On the Implementation of Hydraulic-Interconnected-Suspensions at the Primary Suspension Stage of High-Speed Rail Vehicles

Gioele Isacchi[a]* and Francesco Ripamonti[a].

[a]*Department of Mechanical Engineering, Politecnico di Milano, Milan, Italy*

*Corresponding author, Gioele.isacchi@polimi.it

ORCID

Gioele Isacchi: 0000-0002-4643-677X

Francesco Ripamonti: 0000-0002-0867-5091

Conflicts of Interest

The Authors declare that there is no conflict of interest.

Funding

This research received no specific grant from any funding agency in the public, commercial, or not-for-profit sectors.

Acknowledgements

This study is part of a research project involving Politecnico di Milano and Koni BV. The authors gratefully acknowledge Koni for providing the support and data necessary for this work.

On the Implementation of Hydraulic-Interconnected-Suspensions at the Primary Suspension Stage of High-Speed Rail Vehicles

In recent years, huge investments have been made to improve the dynamic performance of high-speed trains. Research into innovative suspension components has been part of the development of this transport system for decades. Innovative devices can allow rail vehicles to deal with the constantly increasing speed required by the global market.
Among the most innovative suspension layouts proposed in railway dynamics in past years, limited attention has been given to Hydraulic Interconnected Suspensions (HIS). This layout is composed of two hydraulic cylinders with external hydraulic connections. HIS allow promising tuning capabilities due to their ability to offer different responses based on the specific inputs given to the cylinders. This layout is rarely considered for rail vehicles, and the few previous works related to this topic considered the HIS layout to be applied at the secondary suspension stage.
In this context, this paper proposes applying an HIS layout to the primary suspension stage of rail vehicles, in order to overcome the trade-offs between ride comfort, running safety and maximum car body displacement that need to be considered by bogie manufacturers when designing and optimising these mechanical systems. A nonlinear physical model of the HIS is proposed for co-simulation with a Multi-body (MB) model of a high-speed train. The improvement provided implementing an HIS at the primary suspension stage is then compared to similar enhancements that could be made when tuning and varying the standard suspension components of a bogie.

Keywords: hydraulic anti-roll bar; ride comfort; multi-body; wind gust; train dynamics.

1 Introduction

In recent decades, high-speed trains have been offering higher commercial speed in order to improve their competitiveness compared to passenger air transport. As a direct consequence, new challenges are being introduced for passenger trains to match the desired performance in terms of stability, ride comfort and safety. These contemporary issues can be solved by applying research efforts to developing innovative suspension components able to overcome or alleviate the trade-offs that afflict conventional passive solutions.

Smart solutions have been explored for both the primary and secondary suspension stages. Smart primary suspension components have been studied to mainly improve stability and steering performance of rail vehicles[1]. A few exceptions[2,3] are related to semi-active primary vertical dampers that have been successfully applied to high-speed rail vehicles in order to improve their ride comfort performance. Secondary suspension components have generally been proposed to improve ride comfort. For example, the effect of active vertical dampers on ride comfort has been studied numerically[4]. A smart solution has been prototyped and tested to reduce the car body vibrations in rail vehicles[5]. Moreover, lateral semi-active solutions have been proposed to enhance ride quality of rail vehicles operating on tracks with different characteristics[6]. One exception related to the secondary suspension stage is represented by the yaw damper, a component which plays a relevant role in vehicle's stability and curve taking performance[7], as well as ride comfort[8]. In this case, semi-active and active solutions have been studied to increase vehicle stability[9,10] by highlighting their effect on train stability.

Regarding the secondary suspension

stage, an interesting solution is the Hydraulic Interconnected Suspension (HIS). The basic layout of this technology is represented by the interconnection of two cylinders by means of a passive hydraulic circuit, composed of pipes, valves and accumulators. HIS passive configurations are very popular in automotive engineering[11], where this concept has been widely adopted thanks to its capability of decoupling the response of the suspension from vertical and roll excitations[12]. The HIS proved to be a valid solution to improve stability and ride comfort of road vehicles[13]. In railway dynamics, preliminary investigations into this component's capability to offer increased tuning capabilities in passive configuration were reported[14]. Moreover, active interconnected layout combined to active lateral device proved to be a valid solution in the secondary suspension stage of rail vehicles to reduce the perceived lateral acceleration during the negotiation of curves at high speed[15]. Another example of a passive HIS, applied in series to the air bellows of the secondary suspension stage of rail vehicles, obtained a reduction of the car body's vertical acceleration in the frequency range of [1 – 3.3 Hz][16].

In this context, this paper aims to examine the possibility of introducing a passive HIS solution at primary suspension stage of rail vehicles, unlike all the aforementioned works. The HIS can be considered to be valid solution to improving the overall tunability of the primary suspension stage. For this reason, this paper addresses the implementation of an HIS component for each wheelset, replacing the primary vertical dampers. Therefore, the proposed layout is intended to overcome the trade-offs that passive springs and dampers must respect in this suspension stage. For example, it is well known that the primary suspension stage applies an initial filtering effect on the vibration transmitted from the wheels / rails contact to the car body. Their influence on ride comfort has been already cited for hydraulic dampers[2,3] and has further been related to role of primary vertical springs[17], whose stiffness value is inversely proportional to the acceleration perceived on the car body. Moreover, a reduction of the vertical stiffness of the primary suspension stage has been correlated to a reduction in the vibrations transmitted to the ground from rail vehicles[18]. Further correlations between the stiffness of primary vertical springs and wheel wear have been reported[19]. Unfortunately, the design flexibility of the passive elements of the primary suspension stage is limited by the thresholds that must be respected in terms of the maximum allowable displacement of car body (and bogie). In fact, softer primary springs may lead to an increase in car body displacement, especially in critical running conditions such as when negotiating curves and during the response to lateral wind gusts. Therefore, primary vertical stiffness is selected to respect a trade-off between the aforementioned performance levels. In this context, the HIS is intended to offer to bogie manufacturers greater flexibility allowing them to design primary suspension stages able to guarantee running safety and improved ride comfort performance.

This paper is organised as follows: in section 2, the layout of the proposed HIS device is presented. A nonlinear physical model is formulated, together with a virtual characterisation test of the proposed HIS configuration. Then, a Multi-body (MB) model of a test case vehicle is developed. Moreover, two numerical simulations are introduced. They focus on assessing the ride comfort and evaluating the train's response with severe crosswind. In section 3, the influence of the HIS at the primary suspension stage is presented by showing how it can increase design flexibility for the bogie by overcoming the typical design trade-offs of primary vertical suspensions. The dynamic performance indexes of the train during the two simulated scenarios are shown. Finally, section 4 concludes the paper, addressing the future objectives for this kind of suspension component.

2 Methods and Models

Model of the Hydraulic Interconnected Suspension (HIS)

This paper focuses on a new solution based on an HIS layout to be implemented in the primary suspension stage of high-speed rail vehicles. The structure of the proposed device is illustrated in figure 1. The HIS device is composed of two cylinders designed to avoid the oil flow between the upper and lower chambers. These cylinders are intended to replace the train's primary vertical dampers. The HIS has two hydraulic lines: one connects the upper left chamber with the lower right chamber, while the other links the lower left and upper right chambers. For each hydraulic line, an accumulator partially filled with gas is considered. Throttling valves are inserted between the accumulators and lines and in the hydraulic lines in order to simulate energy dissipation within the hydraulic components.

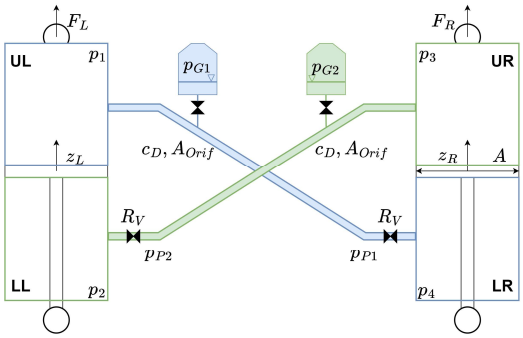

Figure 1 Schematic diagram of the HIS layout. The upper left chamber (UL) is connected to the lower right chamber (LR) through hydraulic line 1, while the hydraulic line 2 connects the upper right chamber (UR) with the lower left chamber (LL).

The behaviour of the HIS component is simulated by means of a nonlinear physical model developed in Matlab/Simulink. The model is based on the formulation of the continuity equation for the chambers of the cylinders and the accumulators, while the fluid in the hydraulic pipes is considered to be uncompressible, as suggested in a previous work[15]. The continuity equations of the upper left chamber (UL), upper right chamber (UR), lower left chamber (LL) and lower right chamber (LR) are reported in equations 1-4 respectively, in which the corresponding oil flows entering from the hydraulic pipes (Q_1 , Q_2 , Q_3 and Q_4) are considered:

$$Q_1 - c_i(p_1 - p_2) - c_e p_1 = \dot{V}_{UL} + \frac{V_{UL}}{\beta}\dot{p}_1 \quad (1)$$

$$Q_2 + c_i(p_1 - p_2) - c_e p_2 = \dot{V}_{LL} + \frac{V_{LL}}{\beta}\dot{p}_2 \quad (2)$$

$$Q_3 - c_i(p_3 - p_4) - c_e p_3 = \dot{V}_{UR} + \frac{V_{UR}}{\beta}\dot{p}_3 \quad (3)$$

$$Q_4 + c_i(p_3 - p_4) - c_e p_4 = \dot{V}_{LR} + \frac{V_{LR}}{\beta}\dot{p}_4 \quad (4)$$

Where the coefficients c_i and c_e indicate the internal and external oil leakages, respectively. The volume of chambers 1 to 4 is described by V_{UL} , V_{LL} , V_{UR} and V_{LR} respectively , and a constant oil bulk modulus β is considered. If we consider the strokes z_L and z_R for left and right cylinders of the HIS respectively, equations 1-4 can be rewritten in the following form:

$$\dot{p}_1 = \frac{\beta}{V_{UL,0} - Az_L}[Q_1 - c_i(p_1 - p_2) - c_e p_1 + \dot{z}_L A] \quad (5)$$

$$\dot{p}_2 = \frac{\beta}{V_{LL,0} + Az_L}[Q_2 + c_i(p_1 - p_2) - c_e p_2 - \dot{z}_L A] \quad (6)$$

$$\dot{p}_3 = \frac{\beta}{V_{UR,0} - Az_R}[Q_3 - c_i(p_3 - p_4) - c_e p_3 + \dot{z}_R A] \quad (7)$$

$$\dot{p}_4 = \frac{\beta}{V_{LR,0} + Az_R}[Q_4 + c_i(p_3 - p_4) - c_e p_4 - \dot{z}_R A] \quad (8)$$

The continuity equation is also formulated for the accumulators mounted on the two hydraulic lines, which present both oil and gas. It can be obtained from the polytropic gas equation and its partial derivative with respect to time. These equations describe the relationship between pressure and volume of a gas medium under different conditions: from a starting (p_{G0}, V_0) to a final condition (p_G , V_G). For each accumulator, they are reported as:

$$p_{G0}V_0{}^{\gamma} = p_G V_G^{\gamma} \tag{9}$$

$$\dot{V}_G = -\frac{V_G^{\gamma}}{\gamma p_G V_G^{\gamma-1}}\dot{p}_G = -\frac{V_G}{\gamma p_G}\dot{p}_G \tag{10}$$

By inverting equation 9 and substituting V_G in equation 10, it is possible to quantify the partial derivative of the gas pressure under the hypothesis of relatively negligible compressible behaviour of the oil compared to the gas. In this way, the differential equations that describe the variation of the gas pressure inside the accumulators are reported in equations 11 and 12, considering oil flows Q_{a1} and Q_{a2} flowing from the accumulators to the corresponding hydraulic pipes.

$$\dot{p}_{G1} = -Q_{a1}\frac{\gamma p_{G1}{}^{\frac{1+\gamma}{\gamma}}}{V_0 p_{G0}{}^{\frac{1}{\gamma}}} \tag{11}$$

$$\dot{p}_{G2} = -Q_{a2}\frac{\gamma p_{G2}{}^{\frac{1+\gamma}{\gamma}}}{V_0 p_{G0}{}^{\frac{1}{\gamma}}} \tag{12}$$

If we take the oil inside the pipes to be incompressible, we can state the continuity equation applied to hydraulic lines 1 and 2 respectively as:

$$Q_{a1} = Q_1 + Q_4 \tag{13}$$

$$Q_{a2} = Q_2 + Q_3 \tag{14}$$

Considering equations 13, we can introduce the dissipative effect of the throttling valve in hydraulic line 1. In literature, different kinds of throttling valves have been applied to HIS prototypes, from shim stack valves[20] to spool valves[21]. These solutions present different relationships between oil volume flow and pressure difference across the valve, and these characteristics are strongly related to their internal layout. Nevertheless, by introducing a simplifying hypothesis based on the presence of an equivalent linear dissipative element (modelled by means of the parameter R_V), the behaviour of disparate technological solutions can be approximated as shown in:

$$Q_4 = Q_{a1} - Q_1 = \frac{1}{R_V}(P_{p1} - p_4) = \\ = \frac{1}{R_V}(p_1 - \Delta_{pipe1} - p_4) \tag{15}$$

where Δ_{pipe1} is the pressure loss along the pipe, that can be expressed by the Darcy formulation under the assumption of laminar flow through the hydraulic line[22], as implemented by some research works[11,23]:

$$\Delta_{pipe1} = \frac{128\rho\nu L Q_4}{\pi d_{pipe}^4} = \\ = \frac{128\rho\nu L(Q_{a1} - Q_1)}{\pi d_{pipe}^4} \tag{16}$$

It is worth mentioning that the hypothesis of linear dissipative elements introduced in equation 15 is proposed in several research works focused on the implementation of interconnected suspensions on different road vehicles[24–26]. Therefore, the overall formulation of the oil flow Q_4 related to hydraulic line 1 can be observed in

$$Q_1 = Q_{a1} - \frac{p_1 - p_4}{R_V\left[1 - \frac{128\rho\nu L}{R_V\pi d_{pipe}^4}\right]} = \\ = Q_{a1} - \frac{p_1 - p_4}{R_V - \frac{128\rho\nu L}{\pi d_{pipe}^4}} \tag{17}$$

According to the same principle, the oil flow Q_3 present in hydraulic line 2 is stated in equation 18.

$$Q_3 = Q_{a2} - \frac{p_3 - p_2}{R_V\left[1 - \frac{128\rho\nu L}{R_V\pi d_{pipe}^4}\right]} = \\ = Q_{a2} - \frac{p_3 - p_2}{R_V - \frac{128\rho\nu L}{\pi d_{pipe}^4}} \tag{18}$$

The last equations required to describe the oil flow entering the hydraulic lines from the accumulators can be obtained under the hypothesis of similar pressure at the top of the chambers and at the inlets to the accumulators. This hypothesis is coherent with a hydraulic layout characterised by relative proximity of

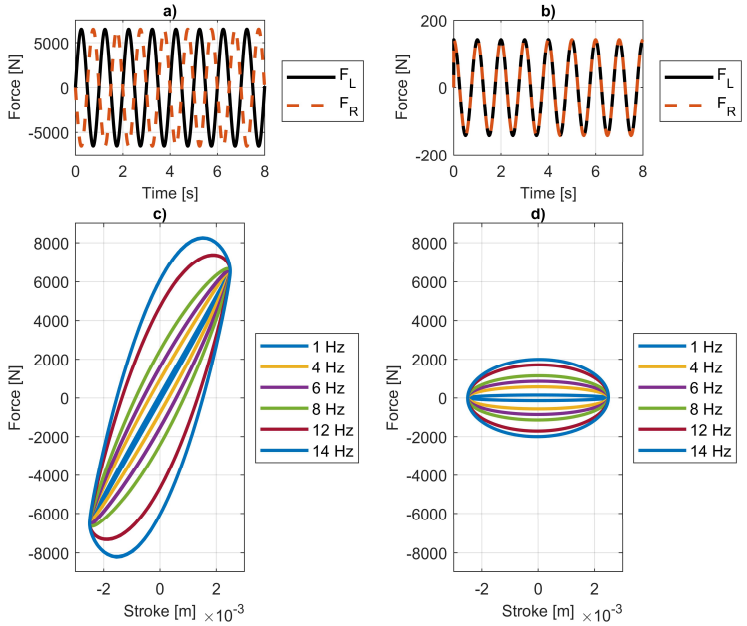

Figure 2 a) Time domain response of the HIS at the first sinusoidal cycle, roll condition. b) Time domain response of the HIS at the first sinusoidal cycle, heave condition. c) Hysteresis cycles provided by the left cylinder to sinusoidal roll cycles. d) Hysteresis cycles provided by the left cylinder to sinusoidal heave cycles.

each gas accumulator to the inlet section of the corresponding upper chamber. Therefore, a negligible pressure variation can be considered by avoiding the presence of any throttling valve between the upper chambers and the corresponding gas accumulators. Therefore, we state that:

$$Q_{a1} = c_D A_{orif} \sqrt{\frac{2(p_{G1} - p_1)}{\rho}} \tag{19}$$

$$Q_{a2} = c_D A_{orif} \sqrt{\frac{2(p_{G2} - p_3)}{\rho}} \tag{20}$$

The overall model of the HIS consists of the continuity equations reported in the differential formulations expressed by equations 1-4 and equations 11,12. They describe the mass conservation in the cylinder chambers and gas accumulators, respectively. In addition, the six oil flows related to the hydraulic pipes are described by equations (13,14,17-20). Additionally, the piston forces imposed by the HIS at left and right positions can be obtained from

$$F_L = A(p_2 - p_1) \tag{21}$$

$$F_R = A(p_4 - p_3) \tag{22}$$

The HIS component generates two forces according to the two different displacement inputs imposed on both the left and right cylinders. Due to its specific layout, the HIS provides different responses according to the relationship between the z_L and z_R strokes. To compare the response of the HIS in different ideal conditions, a set of sinusoidal cycles with 2 mm peak stroke and ascending frequency was imposed on the HIS model. Two working conditions were assessed: a roll and a heave scenario, in which the sinusoidal displacements are applied according to

$$\begin{cases} z_L = A_{cyc} \sin(2\Omega f_{cyc}) \\ z_R = A_{cyc} \sin(2\pi f_{cyc} + \varphi) \end{cases} \tag{23}$$

Where φ is equal to 0 (for heave condition) or π (for roll condition).
In figures 2a and 2b, the forces generated by the left and right cylinders are reported for the roll and heave scenarios, respectively. One can see that the phase shift between inputs z_L and z_R allows the HIS to provide an anti-roll effect due to the combination of F_L and F_R, while in the other case the forces developed by the HIS do not present any relative phase. This peculiarity allows the HIS to act as a hydraulic anti-roll bar when the bogie is subjected to purely roll motions, while the two cylinders act similarly to the primary vertical dampers when the bogie is moving according to a purely vertical motion. In particular, the roll and heave responses of the HIS are compared in figures 2c and 2d. During the roll test, the HIS can provide higher forces than for the heave scenario. Moreover, the roll response is mainly characterised by a significant elastic behaviour especially at low frequency, while a predominantly dissipative effect is provided by the HIS during the heave scenario.

These preliminary results show that the HIS is designed to offer increased roll stiffness to the bogie in order to reduce the roll rotations of the train during severe lateral loads, such as strong gusts of wind and lateral crosswind excitations. At the same time, the hydraulic interconnected layout is implemented to allow decoupling of roll and heave responses and to guarantee higher flexibility and design freedom for bogie manufacturers.

Multi-body model of the railway vehicle

Multi-body analysis proved to be a valid methodology for assessing the influence of different suspension components on the train's dynamics[3,16,27]. For this reason, a MB model of a generic high-speed train is considered as a test-case for assessing the performance of the HIS at the primary suspension stage.

The MB model is developed using Simpack software. It is a single wagon model composed of one car body, two bogies, four wheelsets and eight axle boxes. The model's bodies are all rigid, with the sole exception of the car body. In order to consider the car body's flexibility, a Finite Element (FE) model was created using Abaqus software. Then, the modal dynamics of the car body was introduced into the Simpack MB software. The wheel profile is the S1002CN, and it is coupled with the CN60 rail profile with a rail cant of 1:40, and considering a standard gauge of 1435 mm. A Hertzian approach to the normal direction and the FASTSIM algorithm[28] were implemented to model the contact forces between the wheels and rails. The suspension components were modelled using a linear approach, excepting for the nonlinear hydraulic dampers and nonlinear lateral bump stops. The parameters of the MB model are reported in appendix A. In table 1, the most relevant natural frequencies related to both rigid and flexible modes are reported. It is worth mentioning that the values of the natural frequencies of the test-case model are consistent with those reported in literature for this kind of train[29,30].

Mode shape	Natural Frequency [Hz]
Car body lateral sway	0.65
Car body bounce	0.89
Car body pitch rotation	1.04
Car body yaw rotation	1.13
Car body roll rotation	1.48
Bogie hunting	3.57
Bogie bounce	5.40
Car body flexible diamond mode	9.47
Car body flexible torsion	10.40
Car body first vertical bending	12.07
Car body first lateral bending	14.06

Table 1 *Natural frequencies related to the main mode shapes of the MB vehicle model, evaluated at 350 km/h.*

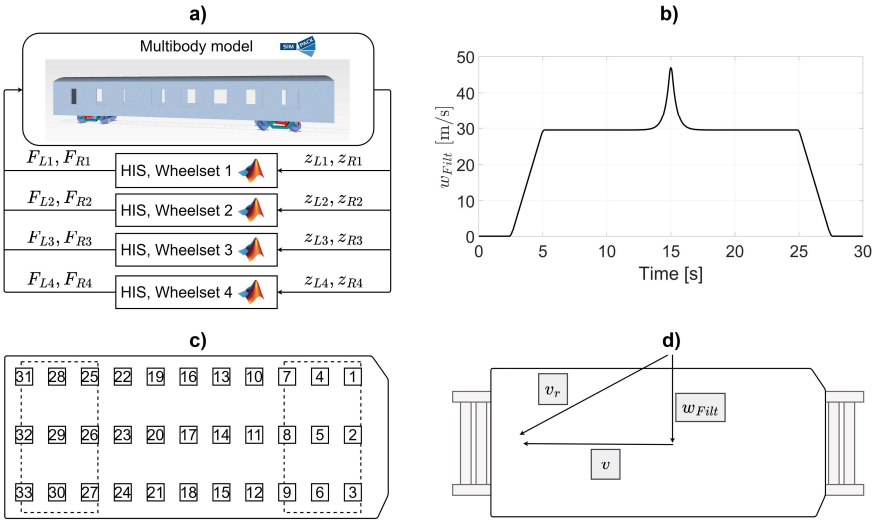

Figure 3 a) Schematic diagram of the SIMAT co-simulation between the Simpack MB model and the four Simulink models for the HIS replacing the primary vertical dampers of the test case train, b) time history of the wind speed profile, c) distribution of the measurement points on the car body floor of the MB model, d) schematic diagram of the wind gust affecting the train during the MB simulation.

The HIS model presented in the previous section is built to be co-simulated with the MB model. In figure 3a, the co-simulation approach is shown. For each wheelset, an HIS device is simulated by means of a Matlab/Simulink model, replacing the suspension elements that simulate the primary vertical dampers. During each step of the co-simulations, the MB model sends the correspondent left and right displacements z_{Li}, z_{Li} to the i − esimal HIS model while the Matlab/Simulink models return the corresponding forces F_{Li} and F_{Ri} to the train model.

Scenario 1: ride comfort assessment

The ride comfort assessment was performed by means of a MB simulation considering a high-speed running scenario. The ride comfort was evaluated according to the Mean Comfort Standard Method proposed in the EN12299 standard, based on the N_{MV} performance index. The test-case train was simulated running on a straight track with a speed of 350 km/h for 300 seconds, as required by the standard. Track irregularity profiles in vertical and lateral directions were considered according to the report ERRI B176/DT 290[31].

The N_{MV} index is a scalar value able to quantify the ride comfort performance for the entire duration of the simulation. It was obtained in the following steps:

- For each direction, a frequency weighted filter was applied to the corresponding acceleration signal to include the human perception of vibrations. The filters applied are those reported in Annex C of EN 12299. The filtered accelerations in longitudinal (x), lateral (y) and vertical (z) directions were obtained.
- The filtered accelerations were divided into windows of 5 seconds, and the Root Mean Square (RMS) value was obtained for each segment in all directions.
- The 95TH percentile of the statistical distribution of the RMS values was

obtained for the three directions: $a_{fx,95}$, $a_{fy,95}$ and $a_{fz,95}$.

- Finally, the N_{MV} was obtained according to:

$$N_{MV} = 6\sqrt{a_{fx,95}^2 + a_{fy,95}^2 + a_{fz,95}^2} \quad (24)$$

The EN 12299 standard requires computing of the N_{MV} index in three different locations on the car body: above the front and rear bogies and at the centre of the wagon. Nevertheless, recent studies suggest improving the robustness of ride comfort assessment by including monitoring of a higher number of measurement locations[32] for instance. For this reason, the post-process procedure proposed in this paper calculates the N_{MV} at 33 different locations on the car body, as show in figure 3c. As a final performance index, the mean index $\overline{N}_{MV}$ is considered.

$$\overline{N}_{MV} = \frac{\sum_{i=1}^{33} N_{MV,i}}{33} \quad (25)$$

Scenario 2: response to a lateral wind gust

The low frequency roll dynamics of the vehicle was studied for this second scenario, focused on the response of the high-speed train to lateral wind gusts. This condition is of great importance for evaluating running safety, since lateral wind gusts can be considered as one of the major causes of derailment[33]. For this reason, a dedicated scenario was simulated by considering a wind load generated by the Chinese Hat Model reported in the Annex I to EN 14067. This wind model can be considered as a robust benchmark for assessing vehicle stability in presence of lateral wind gusts, as reported in previous research work[34]. The wind gust model was generated considering a maximum wind speed of 50 m/s, a severe condition reported several times on Chinese high-speed lines[33]. The wind gust was considered to be perpendicular to the track direction and, as shown in figure 3d, it was filtered according to the standard to obtain the wind speed w_{Filt}, reported in figure 3b as function of time.

The MB simulation represents a straight track running at 350 km/h. In accordance with the standard, track irregularities are not considered. Starting from the wind profile, three external loads are imposed on the centre of mass of the car body: a lateral wind load F_y, a lift load F_y and an overturning moment M_x. They are respectively formulated as:

$$F_y = \frac{1}{2} C_y \rho_{air} h_v l_v v_r^2 \quad (26)$$

$$F_z = \frac{1}{2} C_z \rho_{air} w_v l_v v_r^2 \quad (27)$$

$$M_x = \frac{1}{2} C_m \rho_{air} w_v l_v^2 v_r^2 \quad (28)$$

where $v_r = \sqrt{v^2 + w_{Filt}^2}$ represents the wind speed in relation to the train. The values of the geometrical features of the train, such as height h_v, width w_v and length l_v, and the wind coefficients C_y, C_z and C_m, assumed to be constant, were estimated from other research works[35,36], and are reported in appendix A.

The safety performance of the train during this scenario was assessed by considering the unload index UI suggested in EN 14067. In particular, the index is defined as:

$$UI = \frac{\Delta Q}{Q_0} = 1 - \frac{\sum_{j=1}^{2} Q_{Unloaded}^{j}}{2Q_0} \quad (29)$$

in which the numerator consists of the sum of the dynamic vertical forces on the unloaded wheels of the two wheelsets of a reference bogie. In accordance with EN 14067, the time histories of the vertical forces were low pass filtered considering a 2 Hz cut-off frequency. Besides the safety evaluation, the car body's roll angle θ_c (the rotation of the car body around the longitudinal axis) was taken as a reference index for quantifying the overall displacements of the car body, and for evaluating the anti-roll effects of the HIS device.

3 Results

The HIS device is suggested in this paper to increase the overall performance of the train by allowing greater design flexibility for the

primary suspension stage of the bogie. The train's performance indexes were assessed focusing on ride comfort performance levels ($\bar{N}_{MV}$), obtained from the simulations of scenario 1, and on the performance indexes related to the roll dynamics of the vehicle calculated from the results of scenario 2. In particular, the safety margin is evaluated by means of the maximum value of the unload index of the front bogie and the maximum car body displacement is studied by looking at the maximum value of the roll angle of the car body. The results are reported in two steps:

- First, the typical trade-off to be respected by bogie manufacturers in primary suspension optimisation is presented by comparing the influence on the vehicle's performance of different combinations of the primary vertical springs' stiffness k_{Iz} and damping curve for the primary vertical damper (see figure 4a). In this way, the requirements in terms of ride comfort, running safety and anti-roll performance are assessed.
- Then, the HIS is studied to show how this suspension component can make it possible to overcome the trade-off when combined with a softer setting of the primary vertical springs.

The design of primary vertical suspensions: a trade-off approach

In order to present the trade-off in the design of vertical primary suspensions, the performance of the reference train, the suspension layout of which is described in appendix A, are compared with eight different vehicle layouts consisting of modifications of the primary suspension. This approach introduces variations to the stiffness of the primary suspension springs (k_{Iz}) and the nonlinear damping curve of the primary vertical dampers. In figure 4a, the nine train configurations are summarised. One can see that the eight train types were obtained by varying the standard train layout (Type 5, according to figure 4a) by increasing and decreasing of the nominal values by 50%. Figure 4b shows the 'high damping' and 'low damping' characteristics of the varied layouts.

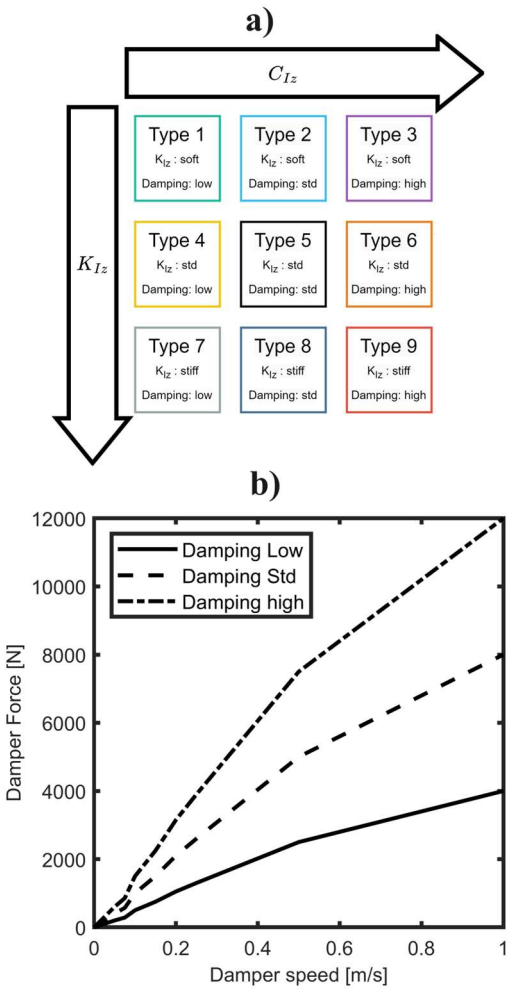

Figure 4 a) train configurations: definition of the nine train types used to study the effect of different values of primary vertical stiffness and primary damping characteristics. b) different damping layout describing the characteristic of the primary vertical dampers considered in the nine train types. Damping 'low' is considered for Types 1,4 and 7; damping 'std' for Types 2,5 and 8 while the 'high' damping setting is implemented in Types 3,6 and 9.

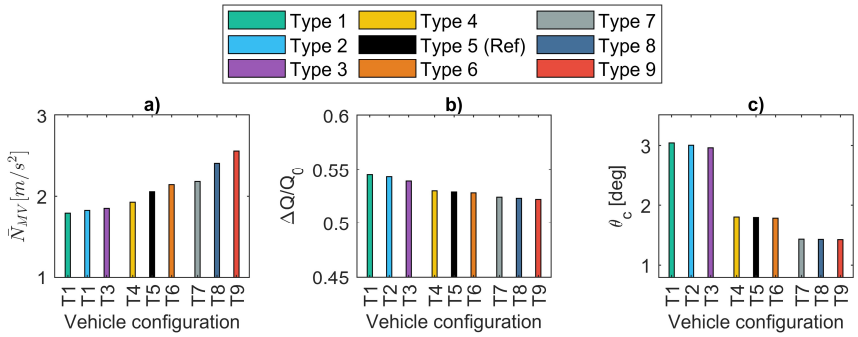

Figure 5 Influence of the stiffness of the primary suspension springs and the damping curve for primary vertical dampers a) on the mean comfort index $\bar{N}_{MV}$, b) on the front bogie UI, c) on the car body roll angle θ_c.

Firstly, the results related to the influence of the different layouts of the vertical suspension elements of the primary stage on ride comfort are studied. In figure 5a, the mean performance index $\bar{N}_{MV}$ obtained from simulating scenario 1 can be seen considering the nine different configurations of the train introduced in figure 4a. The analysis performed on the two parameters shows that:

- Reducing the stiffness of the primary vertical springs has a huge effect on the suppression of the acceleration on the car body perceived by the passengers. Moreover, implementing softer primary vertical dampers induces a parallel positive effect on ride comfort performance.
- The effect of the stiffness of the primary vertical springs on ride comfort is much more relevant than the correspondent effect of the primary vertical dampers.

The results of scenario 2 describe the low frequency dynamics of a train subjected to a lateral wind gust. In figure 5b, the running safety is investigated by comparing the maximum value of the unload index UI for the front bogie (the most critical one). Moreover, in figure 5c the maximum value of the car body roll angle θ_c is compared for the nine train layouts.

From the results reported in figures 5b and 5c, one can see that an increase in primary vertical stiffness k_{Iz} is directly correlated with a reduction in maximum car body displacement, noting the reduced roll angle value reported in figure 5c. At the same time, this improvement is obtained without decreasing safety performance, since the UI is not increased, but slightly reduced. Moreover, the influence of the damping characteristic of the primary vertical dampers is much more limited than that provided by k_{Iz}.

Summarising the results presented in this section, one can see that it is not possible to define a train layout able to improve the three performance indexes presented in this paper simultaneously. Nevertheless, two train layouts can be selected as alternatives to the standard train (Type 5):

- Train Type 1 presents a softer layout of the vertical elements of the primary suspension stage. This configuration can enhance ride comfort performance, but worsens the train's anti-roll behaviour and running safety.
- Train Type 9 is based on a stiffer layout of the vertical elements of the primary suspension stage. This configuration can increase the train's anti-roll capability, reduce the maximum displacements of the car body, and improve running safety. However, this option provides poor ride comfort performance.

Overcoming the trade-off: HIS at primary suspension stage

In this section, an HIS component is proposed to replace the primary vertical dampers and to improve the train's performance, overcoming the trade-off illustrated in the previous section. The MB simulations depicting scenario 1 and scenario 2 are co-simulated with the Matlab/Simulink model of the HIS, and the performance indexes describing the train's dynamics in both conditions are compared with the standard test case train (Type 5) and the two most promising and extreme train layouts selected in the previous section (Type 1 and Type 9). The train configuration considered during the co-simulations is the same as for the previous section, excepting that the primary vertical dampers are replaced by four HIS elements (as shown in figure 3a) and softer settings are used for k_{Iz}, as for the Type 1 configuration. In this way, this approach makes it possible to take advantage of a softer suspension layout, while limiting train motion by means of the additional roll stiffness provided by the HIS device.

In figure 6, a summary of the three performance indexes is reported. In figure 6a, the mean $\bar{N}_{MV}$ index obtained from the simulation of scenario 1 is compared. Figures 6b and 6c report the maximum values of the UI index and the car body roll angle θ_c respectively, obtained from the simulations of scenario 2.

The results are further summarised in figure 7, in which the percentage variations of the performance indexes are reported taking a Type 5 train as a reference.

One can see that the train configuration with HIS at the primary suspension stage and a softer setting of k_{Iz} can provide better performance in both scenarios. The additional stiffness provided by the HIS makes it possible to reduce the characteristic of the primary vertical springs, increasing the filtering effect of the primary suspension stage on vibration transmission from the wheelsets to the car body. The mean $\bar{N}_{MV}$ is reduced by 17.90 %. At the same time, the roll stiffness of the HIS allows the train to reduce the car body angle (-35.62 %) when the high-speed train is subjected to strong lateral wind gusts. These improvements are also correlated to minor enhancement of the safety conditions, quantified by the -3.97 % variation in the UI. It is worth noting that all the performance improvements provided by the combination of a primary HIS and a reduced k_{Iz} are higher than the corresponding ones reached by Type 1 and Type 9. This indicates that the HIS can overcome the trade-off between soft and stiff layouts of the primary suspension stage vertical elements. In

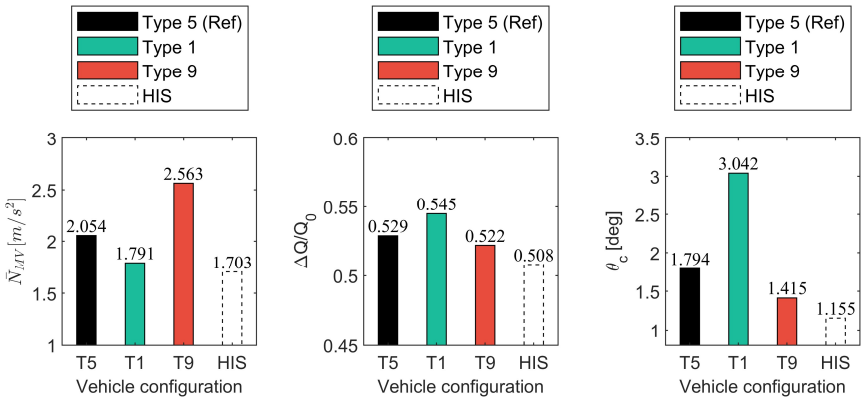

Figure 6 Comparison of train performance levels between standard train layout (Test 5), soft primary suspension setting (Type 1), hard primary suspension setting (Type 9) and a train layout with soft primary vertical spring and HIS replacing primary dampers.

figure 7, the performance indexes are summarised for the three train variations (Type 1, Type 9 and HIS) in terms of both absolute values and variations considering the standard train (Type 5) as reference.

		$\bar{N}_{MV}$ [m/s^2]	UI [\]	θ_c [deg]
Type 5 (standard vehicle)		2.054	0.529	1.794
Type 1	Absolute	1.791	0.545	3.042
	Variation	-12.80%	3.02%	69.57%
Type 9	Absolute	2.563	0.522	1.415
	Variation	24.78%	-1.32%	-21.13%
HIS	Absolute	1.703	0.508	1.155
	Variation	-17.09%	-3.97%	-35.62%

Figure 7 Comparison of the train's performance and related percentage variations compared to the Type 5 setting (standard train).

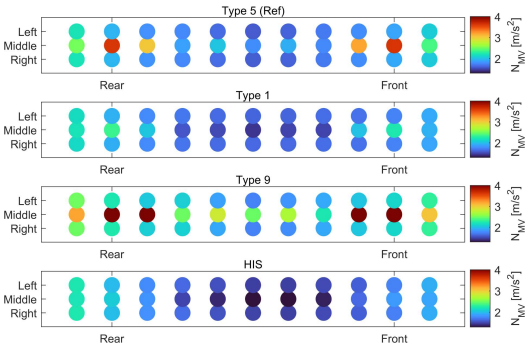

Figure 8 Distribution of the NMV index along the car body floor. Comparison between the reference train (Type 5), a softer layout of the primary vertical suspensions (Type 1), a stiffer layout of the primary vertical suspensions (Type 9) and the implementation of HIS with softer primary vertical springs (HIS).

The ride comfort performance is examined further in figure 8, where the distribution of the N_{MV} index along the car body floor is illustrated for Type 5, Type 1, Type 9 and the train layout with HIS at the primary suspension stage. The HIS can provide a better comfort index distributed over the whole car body. It is interesting to note that excessive levels of vibrations are obtained considering stiffer layouts (such as the Type 9). In particular, the worst locations in terms of ride comfort are located in proximity to the bogies.

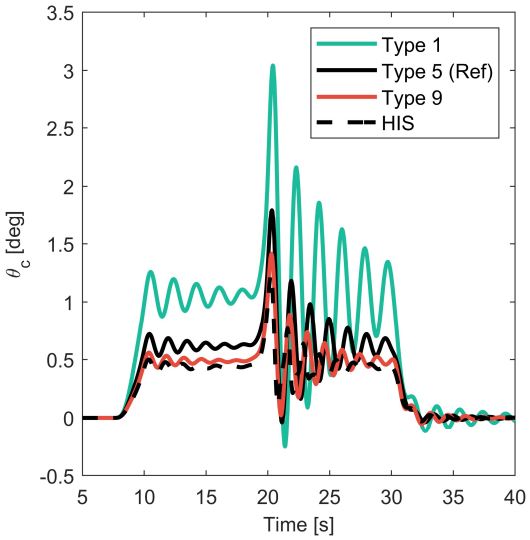

Figure 9 Comparison of the time history of the car body roll angle considering the reference train (Type 5), a softer layout of the primary vertical suspensions (Type 1), a stiffer layout of the primary vertical suspensions (Type 9) and the implementation of HIS with softer primary vertical springs (HIS).

In figure 9, the complete time history of the car body roll angle during the simulation of scenario 2 is reported. The trend is compared between the standard train (Type 5), configurations with softer (Type 1) and stiffer (Type 9) primary vertical suspensions, and the proposed train setup, with HIS replacing the primary vertical dampers. It can be seen that the HIS strongly influences the train's response to the lateral wind gust, leading to a reduction in the car body roll angle, therefore containing the maximum displacement of the train. This reduction is consistent throughout the simulation, leading to smaller peak and average values of θ_c.

4 Conclusions

In this paper, a novel application of a Hydraulic Interconnected Suspension is

proposed for the primary suspension stage of high-speed rail vehicles. The device is intended to replace the primary vertical dampers and to overcome the trade-off that bogie manufacturers must respect when designing the suspension stage. The hydraulic interconnections allow the HIS to offer different response when subjected to roll or heave displacements, providing an additional anti-roll function when the bogie is subjected to purely roll excitations. A nonlinear physical model of the interconnected layout is presented to simulate the response of the HIS. Then, two operating scenarios are defined and simulated by means of a MB approach. The first scenario is focused on the evaluation of the train's ride comfort performance, while the second simulation describes the response of the high-speed train to a strong lateral wind gust.

Before presenting the influence of the HIS on the train's performance, the two scenarios are simulated for nine train configurations consisting of different values of the stiffness of primary vertical springs and different damping curve of the primary vertical dampers. In this way, one of the main trade-offs that influence the design of this kind of mechanical system is presented. In particular, soft vertical suspensions make it possible to improve ride comfort, while deteriorating running safety and increasing the maximum displacement of the car body. On the other hand, stiffer vertical settings of the primary suspensions limit the car body roll angle and provide a minor reduction in the unload index, but introduce a negative effect on ride comfort.

The HIS is then compared with the best train layouts obtained from the previous analysis. It can be combined with soft settings of the primary vertical springs to offer better performance in all aspects of train dynamics, overcoming the trade-off of standard suspension components. In particular, the HIS makes it possible to improve the performance of any other layout, leading to a reduction in the mean ride comfort index $\bar{N}_{MV}$ of about 17 % (during scenario 1) and limiting the maximum car body roll angle of about 35 % (during scenario 2). Moreover, the running safety evaluated in scenario 2 is also slightly enhanced, thanks to a 4 % reduction in the unload index.

In conclusion, the HIS can be considered as a promising layout to be applied at primary suspension stages of high-speed trains, especially considering that this paper demonstrates how the train's performance can be increased with a passive HIS device.

Future research could be focused on the development and characterization of an HIS prototype to investigate the sensitivity of the roll and heave responses to various layouts of both hydraulic line and throttling valves, including also different operating conditions, such as working temperature. Moreover, the upgrade of the proposed layout towards smart solutions (semi-active or active) represents a very interesting next step and would be facilitated by the layout of the HIS device, which could allow the introduction of servo-valves and hydraulic pump. Nevertheless, such advanced solutions should be compared to the passive baseline proposed in this paper by means of cost-benefit analyses.

Conflicts of Interest

The Authors declare that there is no conflict of interest.

Funding

This research received no specific grant from any funding agency in the public, commercial, or not-for-profit sectors.

Acknowledgements

This study is part of a research project involving Politecnico di Milano and Koni BV. The authors gratefully acknowledge Koni for providing the support and data necessary for this work.

References

1. Fu B, Giossi RL, Persson R, et al. Active suspension in railway vehicles: a

literature survey. *Rail Eng Science* 2020; 28: 3–35.

2. Sugahara Y, Takigami T, Sampei M. Suppressing Vertical Vibration in Railway Vehicles through Primary Suspension Damping Force Control. *Journal of System Design and Dynamics* 2007; 1: 224–235.

3. Fu B, Liu B, Di Gialleonardo E, et al. Semi-active control of primary suspensions to improve ride quality in a high-speed railway vehicle. *Vehicle System Dynamics* 2023; 61: 2664–2688.

4. Shi H, Zeng J, Guo J. Disturbance observer-based sliding mode control of active vertical suspension for high-speed rail vehicles. *Vehicle System Dynamics* 2024; 0: 1–24.

5. Ripamonti F, Chiarabaglio A. A smart solution for improving ride comfort in high-speed railway vehicles. *Journal of Vibration and Control* 2019; 25: 1958–1973.

6. Wu Y, Gan F, Shi H, et al. Experimental investigations on the semi-active control of a valve-driven secondary lateral damper for a high-speed rail vehicle. *Journal of Vibration and Control* 2023; 29: 3025–3037.

7. Isacchi G, Ripamonti F. An experimental methodology to support development of yaw damper prototypes based on a hardware-in-the-loop test bench. *Vehicle System Dynamics* 2023; 0: 1–18.

8. Li Y, Chi M, Guo Z, et al. An abnormal carbody swaying of intercity EMU train caused by low wheel–rail equivalent conicity and damping force unloading of yaw damper. *Rail Eng Science* 2023; 31: 252–268.

9. Wang X, Liu B, Di Gialleonardo E, et al. Application of semi-active yaw dampers for the improvement of the stability of high-speed rail vehicles: mathematical models and numerical simulation. *Vehicle System Dynamics* 2022; 60: 2608–2635.

10. Guo J, Shi H, Zeng J. Bifurcation and stability analysis of a high-speed rail vehicle with active yaw dampers. *Journal of Vibration and Control* 2023; 10775463231196272.

11. Qin B, Chen Y, Chen Z, et al. Modeling, bench test and ride analysis of a novel energy-harvesting hydraulically interconnected suspension system. *Mechanical Systems and Signal Processing* 2022; 166: 108456.

12. Smith WA, Zhang N, Hu W. Hydraulically interconnected vehicle suspension: handling performance. *Vehicle System Dynamics* 2011; 49: 87–106.

13. Qi H, Chen Y, Zhang N, et al. Improvement of both handling stability and ride comfort of a vehicle via coupled hydraulically interconnected suspension and electronic controlled air spring. *Proceedings of the Institution of Mechanical Engineers, Part D: Journal of Automobile Engineering* 2020; 234: 552–571.

14. Isacchi G, Nayir FE, Corsi M, et al. Hydraulic interconnected suspension for rail vehicles: a preliminary analysis. *Vibroengineering Procedia* 2023; 50: 91–97.

15. Di Gialleonardo E, Facchinetti A, Bruni S. Control of an integrated lateral and roll suspension for a high-speed railway vehicle. *Vehicle System Dynamics* 2023; 61: 472–498.

16. Luo R, Liu C, Shi H. Dynamic simulation of a high-speed train with interconnected hydro-pneumatic secondary suspension. *Proceedings of the Institution of Mechanical Engineers, Part F: Journal of Rail and Rapid Transit* 2022; 236: 570–581.

17. Wu J, Qiu Y. Modelling and ride comfort analysis of a coupled track-train-seat-human model with lateral, vertical and roll vibrations. *Vehicle System Dynamics* 2022; 60: 2988–3023.

18. Cai Y, Cao Z, Sun H, et al. Effects of the dynamic wheel–rail interaction on the ground vibration generated by a moving train. *International Journal of Solids and Structures* 2010; 47: 2246–2259.

19. Ye Y, Sun Y, Dongfang S, et al. Optimizing wheel profiles and suspensions for railway vehicles operating on specific lines to reduce wheel wear: a case study. *Multibody Syst Dyn* 2021; 51: 91–122.

20. Tan B, Lin X, Zhang B, et al. Nonlinear modeling and experimental characterization of hydraulically interconnected suspension with shim pack and gas-oil emulsion. *Mechanical Systems and Signal Processing* 2023; 182: 109554.

21. Wang B, Zheng M, Zhang N, et al. A comfort performance improved anti-pitch hydraulically interconnected suspension system with switchable dual accumulators. *Proceedings of the Institution of Mechanical Engineers, Part D: Journal of Automobile Engineering* 2023; 237: 2022–2035.

22. Cao D, Rakheja S, Su C-Y. Dynamic analyses of roll plane interconnected hydro-pneumatic suspension systems. *International Journal of Vehicle Design* 2008; 47: 51–80.

23. Zou J, Guo X, Abdelkareem MAA, et al. Modelling and ride analysis of a hydraulic interconnected suspension based on the hydraulic energy regenerative shock absorbers. *Mechanical Systems and Signal Processing* 2019; 127: 345–369.

24. Yang W, Nong Z, Bangji Z, et al. Modeling and performance analysis of a vehicle with kinetic dynamic suspension system. *Proceedings of the Institution of Mechanical Engineers, Part D: Journal of Automobile Engineering* 2019; 233: 697–709.

25. Zhang J, Deng Y, Zhang N, et al. Vibration Performance Analysis of a Mining Vehicle with Bounce and Pitch Tuned Hydraulically Interconnected Suspension. *Chinese Journal of Mechanical Engineering* 2019; 32: 5.

26. Chen S, Zhang B, Li B, et al. Dynamic Characteristics Analysis of Vehicle Incorporating Hydraulically Interconnected Suspension System with Dual Accumulators. *Shock and Vibration* 2018; 2018: e6901423.

27. Isacchi G, Ripamonti F, Corsi M. Innovative passive yaw damper to increase the stability and curve-taking performance of high-speed railway vehicles. *Vehicle System Dynamics* 2023; 61: 2273–2291.

28. KALKER JJ. A Fast Algorithm for the Simplified Theory of Rolling Contact. *Vehicle System Dynamics* 1982; 11: 1–13.

29. Shi H, Wu P. Flexible vibration analysis for car body of high-speed EMU. *J Mech Sci Technol* 2016; 30: 55–66.

30. Sun Y, Zhou J, Gong D, et al. Vibration control of high-speed trains self-excitation under-chassis equipment by HSLDS vibration isolators. *J Mech Sci Technol* 2019; 33: 65–76.

31. Bergander, B., Kunnes, W. *"ERRI B176/DT 290: B176/3 Benchmark Problem, Results and Assessment: Technical Report*. Technical Report ERRI B176/DT 290, European Rail Research Institute, 1993.

32. Palomares E, Morales AL, Nieto AJ, et al. Is the standard ride comfort index an actual estimation of railway passenger comfort? *Vehicle System Dynamics* 2022; 0: 1–14.

33. Montenegro PA, Carvalho H, Ortega M, et al. Impact of the train-track-bridge system characteristics in the runnability of high-speed trains against crosswinds - Part I: Running safety. *Journal of Wind Engineering and Industrial Aerodynamics* 2022; 224: 104974.

34. You W, Kwon H, Park J, et al. Effect of wind gusts on the dynamics of railway vehicles running on a curved track. *Proceedings of the Institution of Mechanical Engineers, Part F: Journal of Rail and Rapid Transit* 2018; 232: 1103–1120.

35. Zhang H, Ling L, Zhai W, et al. An active suspension system for enhancing running safety of high-speed trains under strong crosswind. *Proceedings of the Institution of Mechanical Engineers, Part F: Journal of Rail and Rapid Transit* 2023; 09544097231206216.

36. Bocciolone M, Cheli F, Corradi R, et al. Crosswind action on rail vehicles: Wind tunnel experimental analyses. *Journal of Wind Engineering and Industrial Aerodynamics* 2008; 96: 584–610.

Appendix A: parameters of the MB model of the test-case train

Car body mass	m_c	33630 kg
Car body moments of inertia (x,y,z)	I_{cx}, I_{cy}, I_{cz}	(8.6e4, 1.9e6, 1.9e6) kgm^2
Car body length	l_v	25 m
Car body height	h_v	3.89 m
Car body width	w_v	3.26 m
Bogie mass	m_b	3500 kg
Bogie moments of inertia (x,y,z)	I_{bx}, I_{by}, I_{bz}	(2.0e3, 2.0e3, 3.6e3) kgm^2
Wheelset mass	m_w	1500 kg
Wheelset moments of inertia (x,y,z)	I_{wx}, I_{wy}, I_{wz}	(1.0e3, 0.1e3, 1.0e3) kgm^2
Primary spring stiffness (x,y,z)	k_{Ix}, k_{Iy}, k_{Iz}	(0.3e6, 0.3e6, 1e6) N/m
Secondary spring stiffness (x,y,z)	$k_{IIx}, k_{IIy}, k_{IIz}$	(0.3e6, 0.3e6, 0.3e6) N/m
Wheel radius	R	0.46 m
Secondary roll stiffness	$k_{II,\theta}$	4.1e6 N/m

Wind coefficient, lateral	C_y	0.32
Wind coefficient, lift	C_z	0.22
Wind coefficient, roll	C_m	0.03